Multi-material stereolithography using curing-on-demand printheads

Huachao Mao
School of Engineering Technology, Purdue University, West Lafayette, Indiana, USA
Wenxuan Jia
Department of Aerospace and Mechanical Engineering, University of Southern California, Los Angeles, California, USA
Yuen-Shan Leung and Jie Jin
Epstein Department of Industrial and Systems Engineering, University of Southern California, Los Angeles, California, USA, and
Yong Chen
Department of Aerospace and Mechanical Engineering, University of Southern California, Los Angeles, California, USA and Epstein Department of Industrial and Systems Engineering, University of Southern California, Los Angeles, California, USA

Abstract

Purpose – This paper aims to present a multi-material additive manufacturing (AM) process with a newly developed curing-on-demand method to fabricate a three-dimensional (3D) object with multiple material compositions.

Design/methodology/approach – Unlike the deposition-on-demand printing method, the proposed curing-on-demand printheads use a digital light processing (DLP) projector to selectively cure a thin layer of liquid photocurable resin and then clean the residual uncured material effectively using a vacuuming and post-curing device. Each printhead can individually fabricate one type of material using digitally controlled mask image patterns. The proposed AM process can accurately deposit multiple materials in each layer by combining multiple curing-on-demand printheads together. Consequently, a three-dimensional object can be fabricated layer-by-layer using the developed curing-on-demand printing method.

Findings – Effective cleaning of uncured resin is realized with reduced coated resin whose height is in the sub-millimeter level and improved vacuum cleaning performance with the uncleaned resin less than 10 μm thick. Also, fast material swapping is achieved using the compact design of multiple printheads.

Originality/value – The proposed multi-material stereolithography (SL) process enables 3D printing components using more viscous materials and can achieve desired manufacturing characteristics, including high feature resolution, fast fabrication speed and low machine cost.

Keywords Additive manufacturing, Stereolithography, Multi-material, Printhead, Vacuum cleaning, Printhead

Paper type Research paper

1. Introduction

Enormous demands for multi-material three-dimensional (3D) printing technologies have been identified in application areas, such as research, industry, medical, education and entertainment (Bandyopadhyay and Heer, 2018; Gao *et al.*, 2015; Singh *et al.*, 2019), for the benefit of full-color objects (Sitthi-Amorn *et al.*, 2015), meta-material (Chen and Zheng, 2018), soft material (Truby and Lewis, 2016), composite material (Hamidi and Aslani, 2019; Kokkinis *et al.*, 2015; Papon and Haque, 2019; Yang *et al.*, 2018), functionally graded material (Loh *et al.*, 2018) and four-dimensional (4D) printed material (Deng and Chen, 2015; Kim *et al.*, 2018; Tibbits, 2014). Over the years, many multi-material 3D printing methods have been developed. For example, the multi-jetting deposition modeling (MJM) approach (Sitthi-Amorn *et al.*, 2015) was used to fabricate 3D objects with multiple types of polymers and polymer-derived materials. In the MJM process, a piezoelectric material is used in the printhead to generate a pressure pulse in the fluid, which forces a droplet of ink out from the micro-scale nozzles. Such a deposition-on-demand (DOD) method can jet different material droplets from an array of nozzles to fabricate a 3D multi-material object. This ink-jetting method has been successfully adopted in the industry, such as the "Connex3" printer from Stratasys Inc. It uses the 2D ink-jetting printing technology to deposit droplets of different materials from a large number of nozzles. However, the DOD-based methods have two main drawbacks. First, these methods only apply to liquid resins with low viscosity because more viscous materials, such as oil-like materials, cannot be jetted from the micro-nozzles. Another drawback is the limited reliability because of a large number of nozzles and small nozzle sizes. Also, a higher resolution of the DOD method means a smaller nozzle size,

The current issue and full text archive of this journal is available on Emerald Insight at: **https://www.emerald.com/insight/1355-2546.htm**

Rapid Prototyping Journal

[DOI 10.1108/RPJ-05-2020-0104]

This work was partially supported by NSF grant CMMI 1151191.

Received 25 May 2020
Revised 1 October 2020
19 January 2021
Accepted 26 February 2021

which leads to less reliability, higher cost and fewer material choices.

Besides the multi-ink-jetting deposition method, multi-nozzle fusion deposition modeling (FDM) has also been widely used because of its low cost. FDM uses multiple nozzles to extrude different filament materials and fuses them into a component with multiple materials. However, this multi-nozzle FDM process is applicable only to thermosensitive materials, e.g. acrylonitrile butadiene styrene and polylactic acid; it excludes the commonly used photocurable polymers and the polymer-derived materials (Bagheri and Jin, 2019). Also, the FDM-based 3D printers have limited fabrication speed and surface quality (Armillotta, 2006; Nancharaiah *et al.*, 2010). A variant of the multi-nozzle FDM, known as multi syringes deposition (Truby and Lewis, 2016), is a natural way to deposit soft materials, which finds a large variety of applications to print components with soft matters.

The aforementioned 3D printing processes share the same characteristics, i.e. they use nozzles with different sizes to deposit materials to the demanded area only, as summarized in Figure 1(a)–(c). The difference among these DOD processes is mainly how the material is deposited out of the nozzles. However, a user needs to make trade-offs among the material deposition rate, feature resolution and material choices. In comparison, another widely used additive manufacturing (AM) method, stereolithography (SL), can cure photocurable resin at designated positions using controlled energy input, or "curing-on-demand (COD)." The SL process has become an increasingly used AM process since it was first introduced in 1986 because of its characteristics such as high resolution, fast fabrication speed and extensive material choices (Hull, 1984; Pan *et al.*, 2012; Pan *et al.*, 2012; Tumbleston *et al.*, 2015; Yang *et al.*, 2017, 2019; Zhou *et al.*, 2009). Unlike the DOD methods, COD methods deposit one material on a whole layer regardless of the designed shape, then selectively solidify the material in the area on-demand and, finally, clean the unsolidified liquid resin to prepare to switch to another material. This deposition and cleaning process is repeated for each of the materials to be printed [Figure 1(d) and (e)].

Figure 1 Schematic diagrams of representative multi-material 3D printing processes based on deposition-on-demand and curing-on-demand

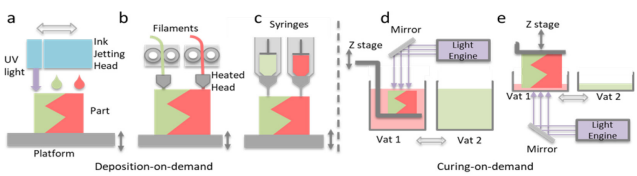

Notes: (a)–(c) Deposition-on-demand processes, where (a) an ink-jetting process uses multiple ink jetting nozzles to deposit materials; (b) an FDM process deposits different thermoplastic filaments; and (c) a syringe-based 3D printing process with different syringes to extrude multiple materials. (d) A two-material top-down SL process, in which the vats with various liquid resins are exchanged, and the uncured resin is cleaned; (e) a bottom-up multi-material SL process – our presented curing -on-demand approach extends this method

Such a COD process, by depositing a whole layer of resin and cleaning the uncured material afterwards, presents different trade-offs among the material deposition rate, feature resolution and material choices. A critical challenge in the COD multi-material SL process is to avoid mixing and contamination between different liquid resins used in the fabrication process. Previous research on multi-material SL processes (Choi *et al.*, 2010, 2011; Inamdar *et al.*, 2006; Kim *et al.*, 2010; Maruo *et al.*, 2001; Wicker *et al.*, 2004) mostly focused on the top-down-based projection, as shown in Figure 1(d). Because the printed part was entirely immersed in the liquid resin, it was difficult to wash and clean the entire printed part before switching the platform to another liquid resin vat. The whole-body cleaning process leads to a large amount of material waste and requires a long washing time.

In comparison, Zhou *et al.* (2013) developed a bottom-up-based multi-material SL process. They used two vats to contain two different liquid resins, and before swapping the material, the uncured resin was cleaned using a brush and an ultrasonic cleaner. Ge *et al.* (2016) presented a similar multi-material printing process, in which two containers with different liquid resins were automatically exchanged to fabricate a part with two materials. Based on the bottom-up projection method, these SL processes need relatively shallower vats of liquid resin; hence, the printed part is immersed in the resin within a limited depth [Figure 1(f)]. Consequently, the uncured resin to be cleaned was significantly reduced to only a few millimeters. Some recent work used dynamic fluidic control of multiple liquid photopolymers for micro-SL (Han, 2019). Regardless, it still requires significant effort and a long time to clean the uncured resin. How to make the coated resin significantly shallower (e.g. in the range of 100 μm) so a more efficient and effective cleaning method can be devised is the main problem addressed in this paper.

To fill the gap in the multi-material SL process development, we herein present a novel 3D printing method based on a new COD printhead, which reduces the coated resin to sub-millimeter level, which is comparable with the layer thickness. The new printhead uses a method of "**c**oating, **c**uring, **c**leaning and **p**ost-curing" (C3P). The core idea of the C3P method is to clean the non-cured material right after selective curing. Specifically, the liquid resin layer is uniformly coated and then selectively photocured using the sliced mask image patterns computed based on the input 3D model. Afterward, the non-cured liquid resin is immediately cleaned up using a vacuum, and any residual resin is further photocured to avoid any potential contamination with other materials. The developed C3P process can enable multi-material printing capability with more material choices and achieve desired manufacturing characteristics such as high feature resolution, fast fabrication speed and low machine cost. In Table 1, we compare our methods with other aforementioned multi-material 3D printing methods. The proposed C3P method has a lower viscosity requirement and is much less expensive than the droplet-on-demand method. Note the speed of "multi nozzles FDM" and "multi syringes extrusion" is dominated by the *XY* translation and extrusion speed, which is much slower than the mask-image-projection-based photocuring. Other COD methods can also cure a whole layer; however, they require a long time to clean uncured liquid resin, which is addressed in the paper.

Table 1 Comparison of our method with other multi-material 3D printing approaches

Methods	Type	Resolution	Speed	Materials	Material viscosity	Cost	Reference
Ink-jetting	DOD	14 μm	Fast	Photo-curable resin	<100 cp	$$	Sitthi-Amorn *et al.* (2015)
Multi-nozzles FDM	DOD	100–200 μm	Slow	Thermo-plastic	–	$	Khalil *et al.* (2005)
Multi-syringes extrusion	DOD	20–200 μm	Slow	Gel-like material	–	$$	Truby and Lewis (2016)
Top-down SL	COD	~30 μm	Slow	Photo-curable resin	<1,000 cp	$$	Choi *et al.* (2011)
Bottom-up SL	COD	~47 μm	Slow	Photo-curable resin	<1,000 cp	$$	Zhou *et al.* (2013)
Our method	COD	30 μm	Medium	Photo-curable resin	<1,000 cp	$$	This paper

Notes: "DOD" means deposition-on-demand, and "COD" indicates curing-on-demand. The "cost" reflects the key components' cost in the corresponding process. The method "Ink jetting" refers to Stratasys J750. The resolution of "DOD" is determined by the nozzle size, whereas the resolution of "COD" is determined by the pixel size of the projection image

The rest of this paper is organized as follows. Section 2 describes the multi-material SL printing process and the related printhead design. Methods to represent a component with multiple materials are discussed in Section 3. Section 4 experimentally characterizes the vacuum cleaning parameters and performance. Various fabrication results are shown in Section 5. Finally, Section 6 concludes the paper with future work.

2. Principle of the C3P-based multi-material stereolithography process

In this section, we present the principle and a related prototype of the proposed multi-material SL process. As mentioned above, the main idea of the C3P process is to effectively clean the non-cured resin right after the selective photocuring. A well-designed printhead is critical to increasing printing efficiency, enhancing resin cleaning performance and eliminating contamination between different materials.

2.1 Process overview

A COD approach was developed in our study to address multi-material coating, resin cleaning and eliminating potential material contamination. Figure 2(a) gives a schematic diagram of the printing system with multiple printheads. The detailed design of the printhead to fulfill the C3P process will be discussed in Section 2.2. Unlike the DOD method, a whole liquid resin layer is coated in C3P regardless of the layer's designed shape. After the resin is coated, the printhead moves toward the curing section, as shown in Figure 2(a). A digital micromirror device (DMD) was used to project a 2D image to the newly coated resin area and selectively cure a thin layer of the resin into the 2D sliced shape. Afterward, the uncured liquid resin will be removed using a vacuum cleaning approach. After the uncured resin is cleaned, the printhead moves further toward the right, and a strong ultraviolet (UV) light post-cures any liquid residue on the part surface before the next printhead moves in. Through the "coating, curing, cleaning and post-curing" process, one material can be successfully deposited onto the printed object mounted on the platform with the designed shape.

After the first printhead finishes its C3P process, a second printhead moves toward the right to start the next C3P process and add the second type of material to the same layer [Figure 2(a)]. When all the printheads finish the C3P printing process of the layer, the printed layer was deposited with multiple materials in controlled shapes. The platform will raise a layer thickness. This procedure will be repeated layer-by-layer to create a 3D object with designed material depositions (refer to a video in the supplementary material).

Figure 2 Schematic diagrams and prototype of the multi-material stereolithography process

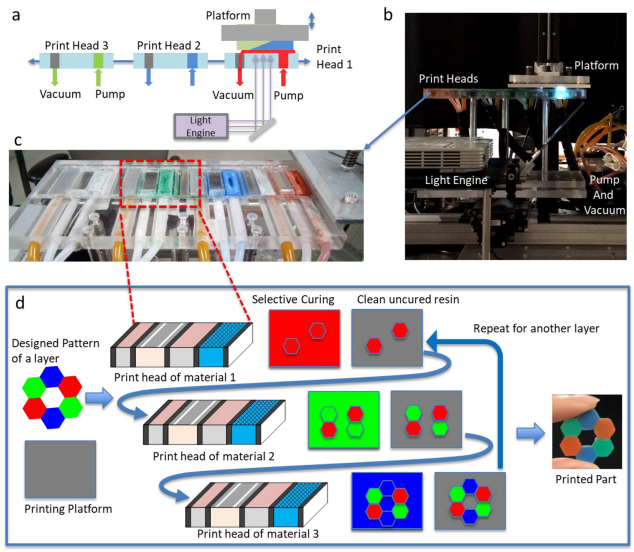

Notes: (a) The schematic diagram of the printing process; (b) a prototype system of the C3P process; (c) the assembly of four printheads to support the printing of four different materials; (d) an illustration of the printing process of a layer using three materials

The developed prototype of the multi-material SL printer is shown in Figure 2(b). The pipes shown in the figure were connected to pumps and a vacuum device, which can coat and clean the resin, respectively. Figure 2(c) displays a prototype of an assembly of four printheads, which can support the 3D printing with four different materials. The rightmost three printheads in Figure 2(c) were used to print an object with red, blue and green resins, whereas the very left printhead was used to print a transparent supporting material. The fabrication process of one single layer with the red, blue and green resins is illustrated in Figure 2(d). The accordingly printed object is also shown in Figure 2(d) (right).

The proposed COD approach has several advantages over the mask-image-projection-based additive manufacturing process described in our previous work (Zhou *et al.*, 2013), which requires several containers with different types of liquid resins. The thorough cleaning of the fabricated parts between different resin tanks is time-consuming and challenging because a large amount of residual resin is left in each container (Zhou *et al.*, 2013). In comparison, the C3P process in this work uses the controlled coating of a small amount of resin, so the material cleaning is more effective and more manageable. Besides, a post-cure procedure after the cleaning step ensures no material contamination between different printheads.

2.2 A Compact printhead with coating, curing, cleaning and post-curing

The core idea of the developed multi-material SL process is to clean a small amount of uncured resin right after selectively curing the desired pattern, and the related printing process would enable a compact printhead design. Consequently, a single linear stage can be used to transport multiple printheads efficiently during the printing process.

Figure 3 shows one designed printhead to fulfill the presented C3P process. The printhead has a flat top, which is divided into four sections – a coating section, a curing section, a vacuum-cleaning section and a post-curing section. Our printhead's design goal is to pump as little resin as possible but still sufficient to recoat the whole layer with a given layer thickness (e.g. 50 or 100 μm). Another design goal is to clean out as much uncured resin as possible right after the layer is selectively photocured.

Figure 3 Schematic diagram of a printhead (c) that fulfills the coating, curing, cleaning and post-curing (C3P) process

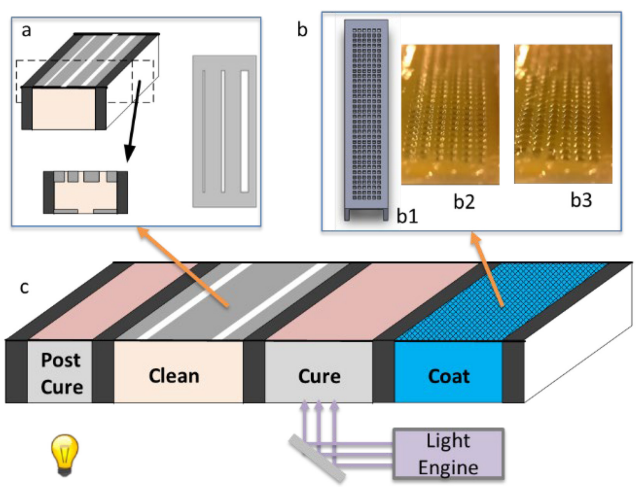

Notes: (a) A cross-sectional view of the vacuum-cleaning section; (b) The design of the coating section (b1) and a close-up view of the fabricated screen mesh with no resin (b2) and with resin permeating the screen mesh with a certain height (b3). Each hole of the screen mesh is 0.7 mm × 0.7 mm, and the hole distance is 1.1 mm in both directions. A transparent glass was used as the top surface of the curing and post-curing sections, so the light from the bottom can penetrate through it

To ensure the printheads have a flat top surface aligned within a layer thickness, we fabricated the four printheads using a whole transparent acrylic sheet with designed slots to pump and vacuum resin. The flat top surface and all the slots of the four printheads were machined together. Hence, the printheads can be directly slid back and forth to swap the deposited resin without the time-consuming move-up-and-down transition (Zhou *et al.*, 2013). The sliding of the printheads also reduces the separation force using the shear force to separate the cured resin from the projection surface, which is smaller than the direct pulling-up force (Pan *et al.*, 2012; Zhou *et al.*, 2013). Notice only the printheads are moved horizontally. The relative position of the projection system and the 3D-printed part are not moved during the sliding process. Hence, the photocuring accuracy of different materials in the layer will not be affected by the switching of resins. Such a linearly moving printhead design enables us to coat the 3D-printed part with liquid resin as shallow as a single-layer thickness. We now discuss the details of these four sections as follows.

2.2.1 Coating

The ideal coating thickness of liquid resin is precisely equal to the fabrication layer thickness (usually between 10 and 250 μm). To achieve this design goal, we develop a novel coating mechanism based on liquid resin's surface tension. In Figure 3(b), a coating screen with designed small holes was used as the coating section's top surface. Because of the liquid's surface tension, the material permeates through the small holes when the liquid pressure reaches a certain level. When the platform passes through the mesh screen from the above, the permeated liquid resin will be coated on the bottom of the previously printed layers and between the gaps. The layer thickness is controlled precisely by the linear Z stage, not by the amount of permeated liquid resin from the mesh screen. By controlling the pump pressure (by adjusting the speed of a stepper motor for the pump), we ensured around 0.3–0.5 mm resin permeated through the mesh screen that was then coated on the previously built layers with a set layer thickness (e.g. 50 or 100 μm). The permeated material height is determined by the surface tension, hole size and liquid resin pressure. Increasing the fluid pressure will increase the permeated resin height [Figure 3(b3)]. In our designed printhead, the pressure can be dynamically controlled by a pump so that the pump settings can adjust the permeated resin height. Therefore, the printhead can control the volume of the coated material, and only a small amount of liquid resin will be coated and used in the curing section. The extra resin will flow into the designed channels between the coating and curing sections [shown as the black area in Figure 3(c)] and suck back to the printhead's resin reservoir.

2.2.2 Curing

After the platform or the previously built layers (including designed supports) are coated with liquid resin slightly higher than the layer thickness, the printhead moves to the curing section and stops there during the curing process. A masked image is then projected upwards through a transparent glass with a coated non-sticky film to the curing section. The coated liquid resin will be photocured according to the projected image pattern. Hence, this photocuring can fabricate the desired shape before the platform moves to the next section.

We used a DMD-based light system to generate the mask image. The DMD contains an array of micromirrors, and each micromirror can be individually switched ON/OFF. Different combinations of the mirrors' ON/OFF states generated the mask images to allow controlled light to pass through a lens group and eventually generated planned projection images on a focusing plane. These focused mask images were used to photocure the coated liquid resin.

A non-sticky film-like polydimethylsiloxane (PDMS) or Teflon film was applied on the curing section's top surface to ensure the newly cured layer can be detached from the printhead and firmly attached to the previously built layers (Chen *et al.*, 2011). Also, because of this non-sticky film's thickness, the curing section's top surface is 100 μm higher than those of the other sections. This height difference ensures only the curing section's top surface directly contacts the built layer after the photocuring process. Other sections' top surface will not directly contact the printed layers during the printheads' linear movement.

2.2.3 Cleaning

Because the printed object may have delicate features, any contact of the photocured layers with the printheads may destroy the newly printed features. A non-contact cleaning approach using a vacuum pump was devised in our study. In the implementation, the "cleaning section" was connected with a vacuum pump via a sealing pipe [Figure 4(a)]. The vacuum pump provides a negative pressure compared to the atmospheric pressure on the section's top surface. Consequently, this negative pressure sucks the uncured liquid resin from the photocured layers.

As shown in Figure 4(a), several small slots of different sizes were designed on the vacuum-cleaning section's top surface. These small slots were designed to increase the vacuum force. Figure 4(b) shows the detailed design of such small slots. The width of the small slots ranged from 50 μm to 1 mm. During the fabrication, the first vacuum slot with a larger size sucked out most of the uncured liquid resin, and then the second and the last slots will further clean the uncured material. The number of such slots could be 1, 2 or more. In our tests, additional slots of more than five slots had little effect on further removing the residual material. After the cured layers passed through the vacuum-cleaning section, most of the uncured material was removed, and only less than 10% residual material was left. The amount of the residual liquid resin on the printed layers is related to the printhead's moving speed; the gap between the vacuum slots and the printed layers; and the vacuum pressure. The cleaning performance of different parameters will be discussed in Section 4.

Figure 4(a) shows the uncured liquid resin is vacuumed into a stopper. Instead of being wasted, the collected liquid resin was recycled into the material reservoir when the stopper's material reached a certain amount. In each printhead, a recycle pump was added to pump the liquid resin in the stopper into the material reservoir. Because a majority of the coated resin is recycled in the printing process, the C3P-based multi-material SL process has much less material waste. It also requires significantly less material swapping time than the cleaning methods of using solvents such as ethanol to wash the uncured liquid resin (Choi *et al.*, 2010; Zhou *et al.*, 2013).

2.2.4 Post-curing

A small amount of residual liquid resin may still exist after the vacuum-cleaning section. To ensure no contamination between different liquid resins when switching to another printhead, we added a post-curing section in the final portion of the printhead. Any residual liquid resin left on the printed layers will be fully cured before it contacts other printheads with different types of resins. This post-curing step can use various kinds of light sources, such as a digital light processing (DLP) projector, a few strong light-emitting diodes and a laser scanning module (Mao *et al.*, 2016). In our implementation of the post-curing section, we reused the DLP light source that was used in the curing section. The post-curing section conducts a second light exposure to the printed layers. The exposure of the residual liquid resin may lead to an additional 10% cured materials (e.g. instead of 100 μm layer thickness, the printed layer will have 110 μm thickness). However, photocuring residual liquid after vacuum-cleaning would ensure no resin contamination between different printheads in the layer-by-layer fabrication process.

Figure 4 Vacuum-cleaning section design

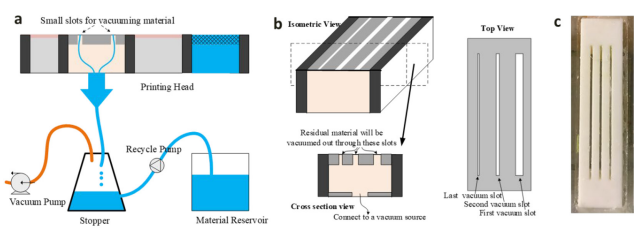

Notes: (a) Illustration of the material cleaning mechanism; (b) the vacuum slot design of a printhead's cleaning section; (c) a fabricated prototype of a vacuum-cleaning section with the same slot size of 700 μm

3. Data representation and process software

This section discusses the data representation and process software developed for the multi-material SL process. We first present the representation method to define a 3D multi-material model and, accordingly, the flow chart to fabricate such a digital model.

3.1 Methods of representing a multi-material model

The input of the developed multi-material SL process is a digital computer-aided design (CAD) model. However, unlike a 3D printing process using a single material, some novel representation methods are required to define a 3D object with multiple material compositions (Leung *et al.*, 2019a, 2019b; Xu *et al.*, 2015). A valid multi-material representation method should uniquely define the material information at any position in the 3D CAD model.

The proposed C3P process requires one mask image for each material at each layer. For this purpose, we used two different model representations in our study:

1 Separate standard triangle languages (STLs) files
An intuitive representation method is to use different STL models to represent each material and then plan the mask image for each printhead accordingly. Each STL model

will be individually sliced into a set of mask images for the layer-based fabrication process (Huang *et al.*, 2013; Zhou *et al.*, 2009).

2 Color images

Our process can also accept a series of color images. The printing process regards each color image as one layer. Given the thickness of each image and the actual size of each pixel, the printer can map the color image to a building range. Four channels of the material information can be extracted from one image's RGB and alpha channels. And each channel information (i.e. red, green and blue) was used to define the mask image for its corresponding printhead.

An example of how a model was represented in the multi-material SL process is shown in Figure 5. For a part defined with three STL models [Figure 5(a)], we first sliced each STL model and reassembled each STL's mask images into a single-color image file (BMP) at each layer. These BMP images represented the material distributions and were used to generate the mask images for each printhead. Besides slicing from the STL models, these digital images can also be directly created using any design packages.

3.2 Software system and process control

We developed a software system using C++ to control the C3P-based multi-material SL process. The software system controls all the devices, including the light engine (a projector with a DMD chip), a vacuum device, four liquid pumps and a three-axis linear stage. The interface of the developed software system is shown in Figure 6(a), and the control logic of the system illustrated as a flow chart diagram is given in Figure 6 (b). On the left side of the diagram, a set of the preparation processes was performed before the actual printing of a 3D object, including configuring the 3D printing system, initializing the platform position and turning on the vacuum and coating pumps. Afterward, the software system executes a printing loop to fabricate the 3D object layer-by-layer, as shown in the middle of Figure 6(b), until all the layers have been printed. The right portion of the flow chart diagram shows the detailed C3P processes for each printhead. And this sub-loop ends when all the printheads finish the C3P process.

Figure 5 An illustrative pipeline of slicing a three-material model to fabricate a multi-material object

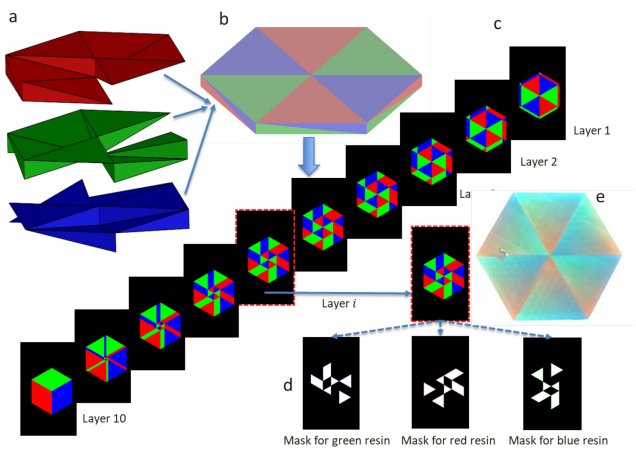

Notes: The given CAD design (b) contains three STL models (a), and each STL model needs to be fabricated with one unique material. All three STL models were sliced using the same layer thickness. The sliced results at each layer were combined to construct a single BMP image. Each RGB channel in the BM Pimages represents one material. The BMP images of all layers are shown in (c). During the fabrication of each layer, the corresponding BMP image's RGB channels will be extracted to form three different projection mask images. An example layer is shown in (d), and each mask image was used to cure the corresponding liquid resin. The 3D-printed object is shown in (e)

Figure 6 System control of the C3P-based multi-material SL process

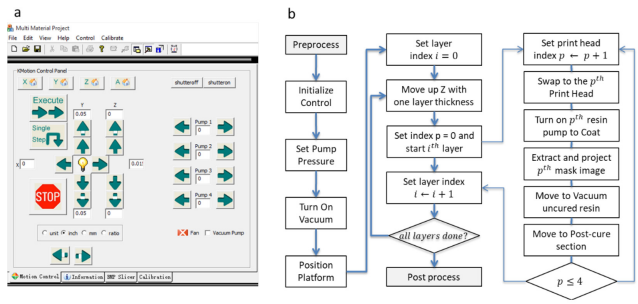

Notes: (a) A developed prototype software system; (b) the control flow chart of the C3P-based multi-material SL process with four printheads

4. Vacuum cleaning characterization and testing

The vacuum-cleaning section in the printhead recycles most of unused liquid resin and determines the Z resolution of the developed C3P-based multi-material SL process. As a critical step in C3P, various experiments were conducted to enhance its cleaning performance.

A vacuum pump was connected to the printheads' vacuum-cleaning sections to remove the uncured liquid resin [Figure 4(a)]. Our experiments showed that the cleaning performance was affected by the relative moving speed between the platform and the printhead; the gap between the printhead and the printed part; and the negative pressure value. Figure 7 (d) and 7(f) presents our experimental results on how these parameters affect cleaning performance. A test part with surface area A was used in our study [Figure 7(c)]. The cleaning performance was measured by the thickness of the residual resin left on the printed part. First, we measured the weight of a clean tissue paper (W_T) using an analytical balance whose resolution is 1 mg. After printing a layer using the printhead, we thoroughly cleaned the printed part using the tissue paper to collect all the residual resin. We then measured the tissue paper to get its weight W_R. Hence, the weight of the residual resin can be calculated as $W = W_R - W_T$, and the total volume of the residual resin can be calculated based on the resin density ρ. Finally, the thickness of the residual resin is $h = W/(\rho A)$.

When the vacuum-cleaning section with opening slots moves close to the built layers with uncured resin, the neighboring air will be sucked into the opening slots because of the pressure

Figure 7 (a) A schematic design of the vacuum-cleaning section. (b) A schematic diagram of the vacuum-cleaning mechanism. (c) A photo of a test part after cleaning uncured resin. No liquid resin can be visually observed. The scale bar is 10 mm. (d)–(f) Height of residual material h_r after cleaning with different process parameters, including (d) the printhead moving speed, (e) the gap between the printed part and the printhead and (f) the negative vacuum pressure. In (d) and (e), the vacuum pressure was set at −180 mmHg; in (e) and (f), the moving speed was set at 3 mm/s and in (d) and (f), the gap was set at 0.1 mm

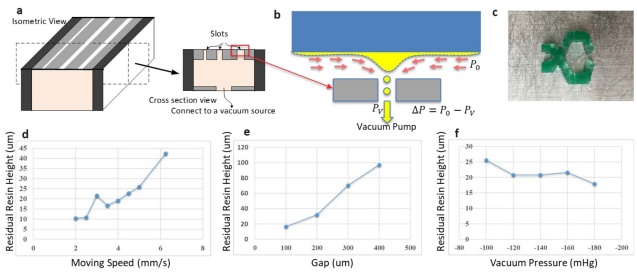

difference [Figure 7(b)]. Consequently, the moving air will bring a certain portion of liquid resin when it moves into the opening slots. When the air moves faster or for a longer time, more liquid resin will be removed from the attached surface. Our experimental data to clean Makerjuice G+ resin is shown in Figure 7(d)–7(f), which verifies the residual material height would decrease when the moving speed decreases, or the gap decreases or the negative vacuum pressure increases. Also, the residual material height as small as 10 μm can be achieved (i.e. ~10% for a 100-μm-layer thickness). The experimental data are consistent with our analysis of the air moving speed and duration. However, it is difficult to derive a quantitative model between the residual resin height with these parameters during the dynamic moving of the vacuum slots. We will study the phenomenon and establish an analytic model in our future research.

To further verify the residual resin height study, small features with two materials interlaced with each other were fabricated. As shown in Figure 8, we successfully built small line features ranging from 200 to 400 μm that were interlaced

Figure 8 Fabrication of interlaced lines with varying sizes using two materials

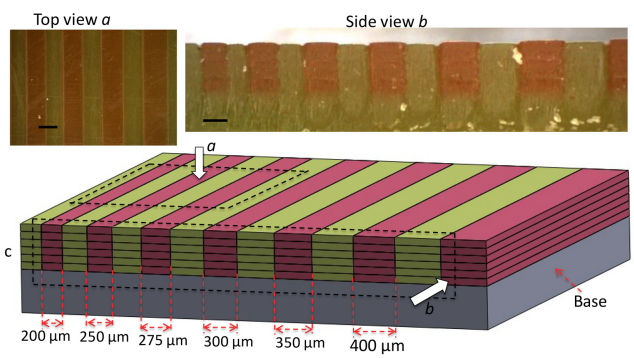

Notes: (a) Top view of the printed lines; (b) side view of multiple layers with the layer thickness of 100 µm; (c) the CAD model of the designed test case. The scale bars are 200 µm

with each other using two types of materials. Figure 8(a) shows the top view of the 3D printed part. Note the last layers of both materials were smooth as the layers were defined by the curing section's constrained film. The residual liquid resin after the curing process is not on the top surface of the layer. Hence, the post-curing of the vacuum-cleaned layers will not affect the surface roughness of the built part. The precise boundary around the small features verifies the cleaning performance of the vacuum-cleaning method. The magnified cross-sectional view [Figure 8(b)] confirms the additional Z height because the uncleaned residual resin is small (within 10 μm). A slight height difference between the two material segments can be observed, which was caused by the misalignment of the printheads for each material. Adjustment based on a better calibration can address the misalignment issue in future research. The small dips between the two material segments were caused by the under-exposure of the boundary pixels between the two neighboring material segments. Better exposure control will also be studied in future research. As shown in Figure 8, although residual resin existed after the vacuum-cleaning sections, the error because of the fully cured residual resin can be barely observable in the printed results after the post-curing sections.

5. Experimental results and discussions

The machine components, motion controllers and materials used in our prototype system are summarized first. The experimental results using the developed system were then presented, followed by a discussion of the limitations and challenges.

5.1 Prototype system and materials

In the constructed prototype, a DLP projector (*Acer H6510BD*) was used. It has a DMD chip with 1920 × 1080 micromirrors to generate mask image patterns. We modified its projection lens, so the image size at the curing plane was 59 mm × 33 mm. An in-house developed C++ software system running on a personal computer (PC) sent a new image pattern to the DLP projector for each layer. The C++ software system also interfaced with a *KFlop* controller (*Dynomotion, Calabasas, CA*) using the USB serial communication. The *KFlop* controller was used to control all the hardware components, including a vacuum device, four liquid pumps and two linear stages for the X- and Z-axes. The vacuum device was switched ON/OFF by using a relay switch to control the power *ON* and *OFF*. The input signal of the relay switch was from a controller's output pin. The four liquid pumps and the two-axis linear stages were all driven by stepper motors. All the six-stepper motors were controlled by the KFlop controller with two *KStep* drivers, which supported eight-axis joint motion.

Two linear stages from Parker (Cleveland, OH) were used to translate the platform that carries the printed part in the Z-axis and the printheads in the X-axis, respectively. The four printheads were assembled on a single frame that was machined from a transparent acrylic plate (from *McMaster Carr*, Santa Fe Springs, CA) using a computer numerical control (CNC) machine. The single machining operation ensures the four printheads' curing sections have the same height (Figure 2).

The coating section's mesh screen window and the cleaning section's slot screen were also CNC-machined (Figure 3). A peristaltic pneumatic pump was used as the resin pump in the coating section of each printhead. The pump was driven by a stepper motor whose speed can be accurately controlled by the *KFlop* controller. A vacuum pump (*ShopVac QSP 20 Gallon* from *McMaster Carr*) was connected to the four printheads' cleaning sections for removing the uncured liquid resin. Note the vacuum pump was shared by the printheads because only one cleaning section will be used at any given time.

The photocurable resin used in our tests was *MakerJucie G+* (with different colors) from *MakerJuice Labs* (Overland Park, KS) that was formulated for 405-nm light. The resin has viscosity 90 cP@20°C, Young's modulus 350 MPa, tensile strength 62.7 MPa, elongation 6% and surface tension 36.5 Dynes/cm. The colors of the liquid resin come from the pigments added to the resin.

5.2 Fabrication results

A set of freeform 3D objects with two or more materials has been fabricated to demonstrate the capability of the developed multi-material SL process. Table 2 shows the typical building time of a layer. The total building time of each layer is 168 s to deposit three materials. Among the building time, the curing time of a layer was 23 s. Note this building time is not related to the part shape nor the number of the parts to be printed because the mask image of a whole layer was projected in the curing process. If a more powerful light bulb was used, the curing time (t_{cure}) could be significantly shortened to a few seconds (Pan *et al.*, 2012). Accordingly, the building time of a layer for three materials could be reduced to ~120 s. Also, the coating time was set to 14 s in our implementation so that liquid resin can be pumped out in the coating section to coat the previously built layers evenly. We believe this coating time could also be largely reduced using a pumping system that is more efficient than the peristaltic pneumatic pump used in our prototype system. Finally, the cleaning and post-curing steps were done simultaneously. That is, during cleaning and post-curing, the printhead was continuously moving forward. The post-curing process will start when only a portion of the part is cleaned and moved into the post-curing section; simultaneously, the rest portion of the part will continue the cleaning process. Hence, there was no delay or clear timing boundary between these two steps; accordingly, we just recorded the total time of these two steps in Table 2.

Figure 9 shows various parts fabricated by the C3P-based multi-material SL process. Figure 9(a) is a test case with a footprint of 30 mm × 30 mm × 1 mm, and its input model was a BMP image with only red and blue pixels to represent two types of materials, respectively. The projection mask for "red material" was formed by extracting all the pixels with red color. In contrast, the projection mask for "blue material" was those pixels with blue color. The actual size of each pixel was set as 30 μm. This test case demonstrates our multi-material printer can support the input representation as a set of color images. Similarly, Figure 9(b) shows a part with three different materials. The input was also a BMP image with red, blue and green colors. Each channel of RGB was extracted to form the mask image to control the deposition of each material. The printed part has a clear boundary between each pair of the two materials provided by the printheads. Figure 9(c) and (d) shows two complex 3D objects with dual materials, respectively. The footprint of the test case in Figure 9(c) is 14 mm × 14 mm × 15 mm, and the test case in Figure 9(d) is a cylinder with a 20 mm perimeter and 2.5 mm height. To fabricate each test case, the input to the printer was two separate STL models. Accordingly, two printheads were used to fabricate this test case, and each printhead was assigned to build one STL model. After each STL was individually sliced, the sliced patterns at the same layer will be assembled into a BMP image with RGB values. When printing, each printhead cured its designed pattern, which was extracted from the assembled images. Figure 9(e) displays a complex example with a footprint of 30 mm × 34 mm × 1 mm. The layer thickness was set at 100 μm, and there were ten layers in total. Because the resin used here (*MakerJuice G+*) was semi-translucent, the light can pass through different layers. The color pattern of the printed part comes from mixing different layers' refractive colors.

Figure 9 Examples of fabricated results. The top row is the input designs, and the bottom row shows the related fabrication results

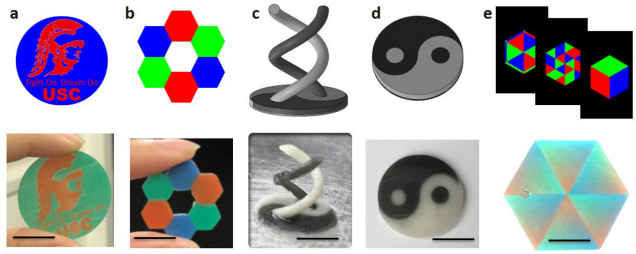

Notes: The inputs of (a) and (b) are BMP images; the inputs of (c) and (d) are STL models designed using SolidWorks; and the input of (e) is a set of images that were computed from three STL models. All the scale bars are 10 mm

5.3 Gradient stiffness using hard and soft materials

The multi-material 3D printing process can fabricate heterogeneous components with the digital material design using a tensor-based error diffusion method (Leung *et al.*, 2019a, 2019b). The designed components with gradient stiffness can then be 3D-printed using the developed multi-material SL system (Figure 10).

Table 2 Building time of one layer (unit: s)

Material 1				Material 2				Material 3				Home	Total
t_{coat}	t_{cure}	t_{clean}	t_{pc}	t_{coat}	t_{cure}	t_{clean}	t_{pc}	t_{coat}	t_{cure}	t_{clean}	t_{pc}	15	168
14	23	14		14	23	14		14	23	14			

Notes: "t_{coat}": coating time; "t_{cure}": curing time, "t_{clean}": cleaning time; and "t_{pc}": post-curing time. "Home" means the time to translate the printheads back to the home position to print the next layer. Notice that "t_{clean}" and "t_{pc}" occur at the same time.

Figure 10 Controlled mixture of two different materials generates gradient stiffness, ranging from a rigid material to a soft material

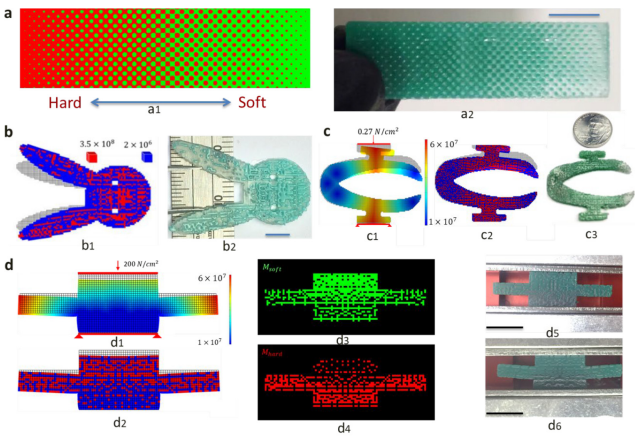

Notes: (a) A digital pattern to transit between two different materials and the as-printed result. (b) A 3D-printed component with designed digital material compositions to achieve non-symmetrical deformations under the same loading force. (c) and (d) Fabrication results of two multi-material designs with complex gradient stiffnesses. Scale bars are 10 mm

Figure 10(a) shows a digital pattern to achieve smooth transit between two different materials. The area with red color indicates a rigid material will be deposited, whereas the area with green color indicates a soft material will be deposited. The rigid material used in our study was MakerJuice G+, with Young's modulus of 350 Mpa; and the soft material was Molecule (Concord, CA) Ra rubber resin, with Young's modulus of 2 Mpa. Figure 10(b) shows a two-material component with a designed digital material distribution to achieve non-symmetrical deformations of the two ears under the same loading force. A stiffness-graded tweezer is shown in Figure 10(c). The tweezer's tip was designed to be soft to grasp fragile objects without breaking them. In Figure 10(c1), the designed Young's modulus distribution shown with red and blue colors indicates rigid and soft materials, respectively. Accordingly, the approximated digital material distribution using only two materials (rigid material with Young's modulus of 350 Mpa and soft material with Young's modulus of 2 Mpa) is shown in Figure 10(c2). The fabricated multi-material tweezer is shown in Figure 10(c3). Finally, another stiffness-graded component is shown in Figure 10(d). Similarly, Figure 10(d1) shows the designed Young's modulus distribution under the given load (200 N/cm^2) and the boundary constraints. Figure 10(d2) shows the approximated material distribution using only two materials. Figure 10(d3) and (d4) shows the mask images used to deposit the hard and soft materials, respectively. Figure 10(d5) is the as-printed part with the designed material composition. When compressed, the 3D-printed object deformed to the shape [Figure 10(d6)] close to the design [Figure 10(d2)]. The digital material design methods were discussed in our previous work (Xu, 2015; Leung *et al.*, 2019a, 2019b).

5.4 Limitations, challenges and future work

Several challenges and limitations need to be addressed in the C3P-based multi-material SL process. First, the vacuum-cleaning section cannot completely clean out the uncured resin in the printhead. In this research, the post-curing step was used to address the issue by fully solidifying the uncleaned resin to ensure no contamination between different printheads. In the future, improved vacuum-cleaning designs and new cleaning mechanisms need to be explored to further reduce the residue resin required in the printhead's post-curing section. Second, the vacuum may stretch or bend the printed small features, especially for those with soft, elastic materials and high aspect-ratios such as small pillars. Figure 10(a) shows a part with 200-μm small features, which were fabricated without problems. For smaller features or ones with a larger aspect-ratio, the effect of feature stretching or bending because of the vacuum will be further investigated in the future study. Third, the bonding between different photocurable resins may be weak. The bonding issue exists in all the multi-material fabrication methods, including the C3P-based method. One potential solution is to optimize the light exposure dosage to maximize the cross-link between different polymers so the bonding strength between different materials can be enhanced. Another approach is to address the bonding issue during the design phase, e.g. using interlock geometries to strengthen the bonding between two different materials.

In addition, some remaining questions to be answered in the future work include:

Q1. How to theoretically analyze the vacuum-cleaning mechanism?

Q2. How to establish the multi-material curing process model to finetune the process parameters?

Q3. How to apply the vacuum-cleaning process to more viscous liquid resin or even composite slurry mixed with ceramic particles, glass or carbon fibers and others?

Q4. What are the killer applications for the multi-material SL process, including the fabrication of functional materials with unique mechanical, optical, magnetic and thermal properties?

6. Conclusions

In this paper, we have presented a novel multi-material SL process using newly developed COD printheads. Each printhead is based on a method of "C3P." The C3P-baed multi-material SL process could enable much more material choices with less restriction on liquid viscosity and achieve desired fabrication characteristics, including high feature resolution, fast fabrication speed and low machine cost. The core idea of the C3P method is to clean the non-cured liquid resin right after the selective photocuring. Because of the printheads' compact design, the C3P process can coat a thin layer of liquid resin; solidify the resin with a single-mask image exposure; clean and recycle the uncured resin using a vacuum device; and eliminate the material contamination because of the residual resin. Several designed parts, including parts with different colors and gradient stiffness, have been fabricated to demonstrate the effectiveness and efficiency of the proposed multi-material SL process. With the feasibility of the COD method demonstrated, further work to improve the cleaning performance, establish the

process models to finetune the process parameters and explore more applications of the multi-material SL process is needed.

References

Armillotta, A. (2006), "Assessment of surface quality on textured FDM prototypes", *Rapid Prototyping Journal*, Vol. 12 No. 1, pp. 35-41.

Bagheri, A. and Jin, J. (2019), "Photopolymerization in 3D printing", *ACS Applied Polymer Materials*, Vol. 1 No. 4, pp. 593-611.

Bandyopadhyay, A. and Heer, B. (2018), "Additive manufacturing of multi-material structures", *Materials Science and Engineering: R: Reports*, Vol. 129.

Chen, D. and Zheng, X. (2018), "Multi-material additive manufacturing of metamaterials with giant, tailorable negative poisson's ratios", *Scientific Reports*, Vol. 8 No. 1, pp. 1-8.

Chen, Y., Zhou, C. and Lao, J. (2011), "A layerless additive manufacturing process based on CNC accumulation", *Rapid Prototyping Journal*, Vol. 17 No. 3, pp. 218-227.

Choi, J.W., Kim, H.C. and Wicker, R. (2011), "Multi-material stereolithography", *Journal of Materials Processing Technology*, Vol. 211 No. 3, pp. 318-328.

Choi, J.-W., MacDonald, E. and Wicker, R. (2010), "Multi-material microstereolithography", *The International Journal of Advanced Manufacturing Technology*, Vol. 49 Nos 5/8, pp. 543-551.

Deng, D. and Chen, Y. (2015), "Origami-based self-folding structure design and fabrication using projection based stereolithography", *Journal of Mechanical Design*, Vol. 137 No. 2, doi: 10.1115/1.4029066.

Gao, W., Zhang, Y., Ramanujan, D., Ramani, K., Chen, Y., Williams, C.B., Wang, C.C.L., *et al.* (2015), "The status, challenges, and future of additive manufacturing in engineering", *Computer-Aided Design*, Vol. 69, pp. 65-89.

Ge, Q., Sakhaei, A.H., Lee, H., Dunn, C.K., Fang, N.X. and Dunn, M.L. (2016), "Multimaterial 4D printing with tailorable shape memory polymers", *Scientific Reports*, Vol. 6 No. 1, pp. 1-11.

Hamidi, F. and Aslani, F. (2019), "Additive manufacturing of cementitious composites: materials, methods, potentials, and challenges", *Construction and Building Materials*, Vol. 218.

Han, D., Yang, C., Fang, N.X. and Lee, H. (2019), "Rapid multi-material 3D printing with projection micro-stereolithography using dynamic fluidic control", *Additive Manufacturing*, Vol. 27, pp. 606-615.

Huang, P., Wang, C.L. and Chen, Y. (2013), "Intersection-free and topologically faithful slicing of implicit solid", *Journal of Computing and Information Science in Engineering*, Vol. 13 No. 2, p. 021009.

Hull, C.W. (1984), "Apparatus for production of three-dimensional objects by stereolithography", available at: www.google.it/patents/US4575330A

Inamdar, A., Magana, M., Medina, F., Grajeda, Y. and Wicker, R. (2006), "Development of an automated multiple material stereolithography machine", *17th Solid Freeform Fabrication Symposium, SFF 2006*, pp. 624-635.

Khalil, S., Nam, J. and Sun, W. (2005), "Multi-nozzle deposition for construction of 3D biopolymer tissue scaffolds", *Rapid Prototyping Journal*, Vol. 11 No. 1, pp. 9-17.

Kim, H., Choi, J.W. and Wicker, R. (2010), "Scheduling and process planning for multiple material stereolithography", *Rapid Prototyping Journal*, Vol. 16 No. 4, pp. 232-240.

Kim, Y., Yuk, H., Zhao, R., Chester, S.A. and Zhao, X. (2018), "Printing ferromagnetic domains for untethered fast-transforming soft materials", *Nature*, Vol. 558 No. 7709, pp. 274-279.

Kokkinis, D., Schaffner, M. and Studart, A.R. (2015), "Multimaterial magnetically assisted 3D printing of composite materials", *Nature Communications*, Vol. 6 No. 1, pp. 1-10.

Leung, Y.S., Kwok, T.H., Mao, H. and Chen, Y. (2019a), "Digital material design using tensor-based error diffusion for additive manufacturing", *Computer-Aided Design*, Vol. 114, pp. 224-235.

Leung, Y.S., Kwok, T.H., Li, X., Yang, Y., Wang, C.C.L. and Chen, Y. (2019b), "Challenges and status on design and computation for emerging additive manufacturing technologies", *Journal of Computing and Information Science in Engineering*, Vol. 19 No. 2, doi: 10.1115/1.4041913.

Loh, G.H., Pei, E., Harrison, D. and Monzón, M.D. (2018), "An overview of functionally graded additive manufacturing", *Additive Manufacturing*, Vol. 23.

Mao, H., Zhou, C. and Chen, Y. (2016), "LISA: linear immersed sweeping accumulation", *Journal of Manufacturing Processes*, Vol. 24, pp. 406-415.

Maruo, S., Ikuta, K. and Ninagawa, T. (2001), "Multi-polymer microstereolithography for hybrid opto-MEMS", *Proceedings of the IEEE Micro Electro Mechanical Systems (MEMS)*, pp. 151-154.

Nancharaiah, T., Ranga Raju, D. and Ramachandra Raju, V. (2010), "An experimental investigation on surface quality and dimensional accuracy of FDM components", *International Journal on Emerging Technologies*, Vol. 1 No. 2, pp. 106-111.

Pan, Y., Zhao, X., Zhou, C. and Chen, Y. (2012), "Smooth surface fabrication in mask projection based stereolithography", *Journal of Manufacturing Processes*, Vol. 14 No. 4, pp. 460-470.

Pan, Y., Zhou, C. and Chen, Y. (2012), "A fast mask projection stereolithography process for fabricating digital models in minutes ", *Journal of Manufacturing Science and Engineering*, Vol. 134 No. 5, doi: 10.1115/1.4007465.

Papon, E.A. and Haque, A. (2019), "Fracture toughness of additively manufactured carbon fiber reinforced composites", *Additive Manufacturing*, Vol. 26, pp. 41-52.

Singh, R., Kumar, R., Farina, I., Colangelo, F., Feo, L. and Fraternali, F. (2019), "Multi-material additive manufacturing of sustainable innovative materials and structures", *Polymers*, Vol. 11 No. 1, p. 62.

Sitthi-Amorn, P., Ramos, J.E., Wang, Y., Kwan, J., Lan, J., Wang, W. and Matusik, W. (2015), "MultiFab: a machine vision assisted platform for multi-material 3D printing", *ACM Transactions on Graphics*, Vol. 34 No. 4, pp. 1-11.

Tibbits, S. (2014), "4D printing: multi-material shape change", *Architectural Design*, Vol. 84 No. 1, pp. 116-121.

Truby, R.L. and Lewis, J.A. (2016), "Printing soft matter in three dimensions", *Nature*, Vol. 540 No. 7633.

Tumbleston, J.R., Shirvanyants, D., Ermoshkin, N., Janusziewicz, R., Johnson, A.R., Kelly, D., Chen, K., *et al.* (2015), "Continuous liquid interface production of 3D objects", *Science*, Vol. 347 No. 6228, pp. 1349-1352.

Wicker, R., Medina, F., Elkins, C. (2004), "Multiple material micro-fabrication: extending stereolithography to tissue engineering and other novel applications", *Proceedings of 15th* . . ., pp. 754-764.

Xu, H., Li, Y., Chen, Y. and Barbič, J. (2015), "Interactive material design using model reduction", *ACM Transactions on Graphics*, Vol. 34 No. 2, pp. 1-14.

Yang, Y., Chen, Z., Song, X., Zhang, Z., Zhang, J., Shung, K. K., Zhou, Q., *et al.* (2017), "Biomimetic anisotropic reinforcement architectures by electrically assisted nanocomposite 3D printing", *Advanced Materials*, Vol. 29 No. 11, p. 1605750.

Yang, Y., Li, X., Chu, M., Sun, H., Jin, J., Yu, K., Wang, Q., *et al.* (2019), "Electrically assisted 3D printing of nacre-inspired structures with self-sensing capability", *Science Advances*, Vol. 5 No. 4, doi: 10.1126/sciadv.aau9490.

Yang, Y., Song, X., Li, X., Chen, Z., Zhou, C., Zhou, Q. and Chen, Y. (2018), "Recent progress in biomimetic additive manufacturing technology: from materials to functional structures", *Advanced Materials*, Vol. 30 No. 36, p. 1706539.

Zhou, C., Chen, Y. and Waltz, R.A. (2009), "Optimized mask image projection for solid freeform fabrication", *Journal of Manufacturing Science and Engineering*, Vol. 131 No. 6, p. 061004.

Zhou, C., Chen, Y., Yang, Z. and Khoshnevis, B. (2013), "Digital material fabrication using mask image projection based stereolithography", *Rapid Prototyping Journal*, Vol. 19 No. 3, pp. 153-165.

Corresponding author

Yong Chen can be contacted at: yongchen@usc.edu